Journal of Computational Physics **177,** 313–335 (2002)
doi:10.1006/jcph.2002.6997, available online at http://www.idealibrary.com on IDEAL®

High-Order Harmonic Spectral Filter with the Double Fourier Series on a Sphere

Hyeong-Bin Cheong,[1] In-Hyuk Kwon, Tae-Young Goo, and Myeong-Joo Lee

Department of Environmental Atmospheric Sciences, Pukyong National University, 599-1 Daeyeon 3-dong, Nam-gu, Pusan 608-737, Korea
E-mail: hbcheong@pknu.ac.kr

Received May 30, 2001; revised December 7, 2001

A high-order harmonic spectral filter (HSF) is implemented to smooth out a field variable defined on a spherical surface using the double Fourier series (DFS) as orthogonal basis functions. The filter consists of the solution of the high-order harmonic diffusion equation with the implicit method, where the high-order harmonic operator is split into second- or lower-order harmonic operators. The second-order harmonic operator is replaced by a pentadiagonal matrix whose elements are the spectral coefficients. First, a biharmonic spectral filter (BiHSF), the prototype of the high-order HSF, is developed where only the second-order harmonic operator is included. It is found that the computational error for the inversion of a pentadiagonal matrix remains in the order of machine rounding. Compared to the mixed-order HSF with DFS used in the previous study, which contains the second- and third-order harmonic operators, the BiHSF can provide a sharper cutoff of high wavenumbers as well as improved computational efficiency. These advantages come from the fact that for each set of spectral coefficients the BiHSF needs only a single inversion of the pentadiagonal matrix whereas the mixed-order HSF requires triple inversions and an auxiliary operation of the tridiagonal matrix. Based on the BiHSF, the high-order HSF up to the sixth order, which is composed of a multiple inversion of tri- or pentadiagonal matrices, is designed. Tests with the rotated Gaussian fields revealed that the HSF with DFS is isotropic. Application to various problems, including a time-dependent strongly nonlinear case and the observed flow, indicates that the high-order HSF is well capable of smoothing out selectively high-wavenumber components without significantly affecting the conserved quantity, such as total (kinetic) energy.

Key Words: high-order harmonic spectral filter; biharmonic spectral filter; double Fourier series; smoothing; inversion of pentadiagonal matrix.

[1] Fax: +82-51-620-6286.

0021-9991/02 $35.00

1. INTRODUCTION

A spectral method with the double Fourier series (DFS) as orthogonal basis functions was developed by Cheong [1, 2] for the solution of shallow-water equations on a spherical surface. It requires $O(N^2 \log N)$ operations per time step with the memory of $O(N^2)$ elements, where N is the spectral truncation. It was demonstrated that a mixed-order harmonic spectral filter (HSF) can stabilize the time integration of nonlinear equations by smoothing out effectively the high-wavenumber components without affecting the physics of the flow. The filter (hereafter referred to as filter type-IIA) includes the second- and third-order horizontal Laplacian (i.e., sixth-order differential equations) and performs spectral smoothing in terms of triple inversions of the Helmholtz equation and a single forward operation of the Laplacian (that is, actually quadruple inversions),

$$[1 - \gamma \nabla^2]^3 Q^f = [1 - 3\gamma \nabla^2] Q, \tag{1.1}$$

where Q^f (Q) is the variable filtered (to be filtered) and γ is the filter coefficient. The application of filter type-IIA to a variable in the spectral space needs computational operations much less than those involved in either the forward or inverse Fourier transform of a variable, by a factor of nearly one order for the moderate resolution of the model. Therefore, use of the spectral filter in (1.1) does not reduce the computational efficiency of the spectral method with DFS, whereas the spherical harmonics filter in [1, 9] requires more operations than is needed for spectral transform (see [3] for an efficient spherical harmonic filter). Though it has been designed for numerical experiments on time-dependent flows, the filter in (1.1) can also be used for a variety of problems, as long as they concern the spectral filtering (smoothing) of a variable on a spherical surface.

In addition to computational efficiency, the choice of filter type-IIA has another advantage, particularly in the case of numerical simulation of time-dependent flows: The filter uses the same tridiagonal matrices, without modification, as those required for the solution of diagnostic equations, such as the relation between the vorticity (divergence) and streamfunction (velocity potential). However, this, in turn, makes it necessary to introduce an auxiliary operation, that is, the Laplacian on the right-hand-side of (1.1).

A question is raised whether such multiple inversions of the Helmholtz equation as well as the auxiliary operation, which constitute the spectral filter in (1.1), are able to provide optimal performance on selective dampening at small scales or high wavenumbers. In other words, the sharp cutoff that could be achieved by incorporation of high-order harmonics might be lost at the expense of numerical convenience. Furthermore, it is certain that the design of high-order HSFs necessitates the auxiliary operation on the right-hand-side (i.e., as a forcing term of the elliptic filter-equation) unless some algorithms other than tridiagonal matrix inversion are developed. This motivates us to look for a high-order HSF that performs filtering through direct inversions of high-order harmonic operators without an auxiliary operation. Such a filter could be produced by splitting the high-order harmonic operators into the second-order or lower harmonic operators, and thus constructing a pentadiagonal matrix for them as we usually construct a tridiagonal matrix for the harmonic operator (i.e., the second-order differential equations). The first step toward the high-order HSF must be constructing a biharmonic spectral filter (BiHSF) in terms of pentadiagonal matrices because it does not require prehandling (i.e., splitting) of the biharmonic filter operator.

In needs of computational stability, global weather and climate models which do not use the spherical harmonics expansion should incorporate a filter or a viscosity [6, 7, 9, 10, 11]. The spherical harmonics model also needs such a stabilizer to prevent the spectral blocking caused by truncation in cases where time-stepping of a strongly nonlinear flow is carried out [4, 5, 8]. Selective damping at small scales is accomplished either by incorporating high-order Laplacian operators into the filter or viscosity [6, 7, 10], or by giving a weight function with a sharp cutoff to the spherical harmonics coefficients [11]. Although the Boyd–Vandeven filter of Taylor *et al.* [11] formally mimics the implicit diffusion, it is not based on the Laplacian operator. For numerical models, except for the spherical harmonics model, there has been no filter that inverts the high-order harmonic operator without decomposing it into harmonic operators [2]. Thus, the approach in this study brings additional advantages to the spectral method with the DFS which are not available in other methods.

This paper is organized as follows. A numerical procedure for the construction of the BiHSF or pentadiagonal matrices with the DFS [1] is presented in the next section. Since the BiHSF is considered a prototype of the high-order HSF in the sense that it provides a basis for a higher order HSF, the derivation is described in some detail. Extension to the high-order HSF with order up to 6, i.e., $[1 + \gamma(-1)^q \nabla^{2q}]Q^f = Q$ with $q = 2, \ldots, 6$, is given in Section 3. Accuracy and performance of the filters are discussed in Section 4 by applying them to various problems which are either static or time-dependent. We present the summary and conclusions in the final section.

2. BIHARMONIC EQUATIONS AND PENTADIAGONAL MATRICES (BIHARMONIC SPECTRAL FILTERS)

2.1. Poisson's Equation on a Sphere and the Double Fourier Series

Since the HSF in this paper is an extension of [1, 2], we begin with a brief description of the method of [1] for the solution of Poisson's equation. Poisson's equation on a sphere of unit radius is given as

$$\nabla^2 w = g(\lambda, \phi), \tag{2.1a}$$

$$\nabla^2 \equiv \frac{1}{\sin\phi}\frac{\partial}{\partial\phi}\sin\phi\frac{\partial}{\partial\phi} + \frac{1}{\sin^2\phi}\frac{\partial^2}{\partial\lambda^2}, \tag{2.1b}$$

where $g(\lambda, \phi)$ is the forcing function, λ is longitude, and $\phi = \pi/2 +$ latitude. Equation (2.1a) is multiplied by $\sin^2\phi$ to facilitate the derivation of tridiagonal matrices when it is expanded using the double Fourier series,

$$[\sin^2\phi]\nabla^2 w = g(\lambda, \phi)\sin^2\phi. \tag{2.2}$$

As in [1, 2], the truncated double Fourier series is introduced for the spectral method; for example,

$$g(\lambda, \phi) = \sum_{m=0}^{M}[g_{-m}(\phi)\cos m\phi + g_m(\phi)\sin m\phi], \tag{2.3}$$

$$g_m(\phi) = \begin{cases} \sum_{n=0}^{N} g_{n,m} \cos n\phi & \text{for } m = 0, \quad (2.4a) \\ \sum_{n=1}^{N} g_{n,m} \sin n\phi & \text{for odd } m, \quad (2.4b) \\ \sum_{n=1}^{N} g_{n,m} \sin\phi \sin n\phi & \text{for even } m(\neq 0), \quad (2.4c) \end{cases}$$

where $g_{n,m}$ is the spectral coefficients of $g(\lambda, \phi)$, and M and N are the spectral truncations. Divided into the symmetric and antisymmetric mode for meridional direction, Poisson's equation is replaced by algebraic equations for each set of spectral coefficients (i.e., for the symmetric and antisymmetric mode of zonal wavenumber m separately) as

$$D\boldsymbol{w} = A\boldsymbol{g}, \tag{2.5}$$

where the matrices D and A are tridiagonal matrices each with the size $N/2 \times N/2$, except for the symmetric mode of the zonal-mean component. A detailed procedure for the construction of the tridiagonal matrices D and A are shown in [1] and are not reproduced here. The column vectors $\boldsymbol{w}$ and $\boldsymbol{g}$ with $N/2$ elements consist of spectral coefficients for $w(\lambda, \phi)$ and $g(\lambda, \phi)$, respectively. For the symmetric mode of $m = 0$, all equations associated with the filter are solved by the use of the Legendre polynomial expansion shown in [2].

2.2. Pentadiagonal Matrices for the Implicit Biharmonic Diffusion Equation

The filter under consideration in this section (referred to as filter type-II) is the implicit biharmonic diffusion equation, defined as

$$[1 + \gamma\nabla^4]w = g(\lambda, \phi), \tag{2.6}$$

where $\gamma(>0)$ is the filter viscosity, $w(\lambda, \phi)$ is the filtered variable, and $g(\lambda, \phi)$ is the forcing function. As before, to facilitate the derivation of band-diagonal matrices associated with the discrete system, Eq. (2.6) is multiplied by $W_A(\equiv\sin^4\phi)$,

$$\sin^4\phi[1 + \gamma\nabla^4]w = g(\lambda, \phi)\sin^4\phi. \tag{2.7}$$

The biharmonic equation above can be replaced by the matrix equation with the double Fourier expansion in (2.4), in a way similar to that for Poisson's equation,

$$Z\boldsymbol{w} = S\boldsymbol{g}, \tag{2.8a}$$

$$S \equiv A^2, \tag{2.8b}$$

where the matrices Z and S must be pentadiagonal, as is shown below. The elements of matrices Z and S can be computed by directly substituting the double Fourier series expansion into the differential operators included in (2.6). Let $w_m(\phi)$ and $g_m(\phi)$ be the zonal Fourier transform, respectively, as in (2.3). Then, Eq. (2.7) is rewritten as

$$[W_A + \gamma(W_D - m^2W_S - m^2W_L + m^4)]w_m(\phi) = [W_A]g_m(\phi), \tag{2.9}$$

where the differential operators are

$$W_D = \sin^3\phi\frac{\partial}{\partial\phi}\sin\phi\frac{\partial}{\partial\phi}\frac{1}{\sin\phi}\frac{\partial}{\partial\phi}\sin\phi\frac{\partial}{\partial\phi}, \tag{2.10a}$$

$$W_S = \sin^3\phi \frac{\partial}{\partial\phi} \sin\phi \frac{\partial}{\partial\phi} \frac{1}{\sin^2\phi}, \tag{2.10b}$$

$$W_L = \sin\phi \frac{\partial}{\partial\phi} \sin\phi \frac{\partial}{\partial\phi}. \tag{2.10c}$$

Representing $w_m(\phi)$ and $g_m(\phi)$ with half-ranged Fourier expansion in (2.4), we can replace (2.9) with a set of linear algebraic equations identical to those in (2.8a). Details of the derivation of them are shown below.

2.2.1. *For Odd* $\boldsymbol{m}$

The differential operators in (2.10) consist of successive differentiation with respect to ϕ and multiplication or division by $\sin\phi$. Derivation of the spectral expansion for the fourth-order meridional differentiation (a part of this is illustrated in the Appendix) yields

$$\begin{aligned}
[W_D]w_m(\phi) &\equiv \sin^3\phi \frac{\partial}{\partial\phi} \sin\phi \frac{\partial}{\partial\phi} \frac{1}{\sin\phi} \frac{\partial}{\partial\phi} \sin\phi \frac{\partial}{\partial\phi} \left[\sum_{n=1}^{N} w_{n,m} \sin n\phi \right] \\
&= \sum_{n=1}^{N} [B_1(n) w_{n-4,m} - B_2(n) w_{n-2,m} + B_3(n) w_{n,m} \\
&\quad - B_4(n) w_{n+2,m} + B_5(n) w_{n+4,m}] \sin n\phi,
\end{aligned} \tag{2.11}$$

where the polynomials attached to the spectral components are

$$\begin{aligned}
B_1(n) &= [(n-4)^2(n-3)^2]/16, \\
B_2(n) &= [(n-4)(n-3)^2(n-2) + (n-3)(n-2)(n-1)(n) \\
&\quad + (n-2)^2(n-1)^2 + (n-2)^2(n-1)(n+1)]/16, \\
B_3(n) &= [(n-3)(n-1)(n)^2 + (n-2)(n-1)^2(n) \\
&\quad + (n-2)(n-1)(n)(n+1) + (n+2)(n+1)(n)(n-1) \\
&\quad + (n+3)(n+1)(n)^2 + (n+2)(n+1)^2(n)]/16, \\
B_4(n) &= [(n+4)(n+3)^2(n+2) + (n+3)(n+2)(n+1)(n) \\
&\quad + (n+2)^2(n+1)^2 + (n+2)^2(n+1)(n-1)]/16, \\
B_5(n) &= [(n+4)^2(n+3)^2]/16.
\end{aligned} \tag{2.12}$$

The differential operator W_L is the same as one of those in (2.2), and the procedure can be found in [1]. Operators for the terms $W_S + W_L$ and W_A result in

$$\begin{aligned}
[W_S + W_L]w_m(\phi) &\equiv [W_S + W_L] \sum_{n=1}^{N} w_{n,m} \sin n\phi \\
&= \sum_{n=1}^{N} [E_1(n) w_{n-2,m} - E_2(n) w_{n,m} + E_3(n) w_{n+2,m}] \sin n\phi,
\end{aligned} \tag{2.13}$$

$$E_1(n) = [(n-4)(n-3) + (n-2)(n-1)]/4,$$
$$E_2(n) = [(n-3)(n+2) + (n+3)(n-2) + 2n^2]/4,$$
$$E_3(n) = [(n+4)(n+3) + (n+2)(n+1)]/4,$$

$$[W_A]w_m(\phi) = \frac{1}{16}\sum_{n=1}^{N}[w_{n-4,m} - 4w_{n-2,m} + 6w_{n,m} - 4w_{n+2,m} + w_{n+4,m}]\sin n\phi. \quad (2.14)$$

For the expansions on the right-hand-side of (2.11)–(2.14), the spectral coefficients with negative indices must be changed into positive indices as

$$\begin{aligned} w_{-3,m} &\to (-w_{3,m}),\\ w_{-2,m} &\to (-w_{2,m}),\\ w_{-1,m} &\to (-w_{1,m}),\\ w_{0,m} &= 0, \end{aligned} \quad (2.15)$$

which follows the inverse transform of (2.4), and the last one is given by definition. We discard the spectral components with indices greater than the truncation, i.e., $w_{n,m} = 0$ for $n > N$.

2.2.2. *For Even* $\boldsymbol{m}(\neq 0)$

As in Cheong [1], both sides of (2.9) are divided by $\sin\phi$ for the use of fast Fourier transform; then the substitution of (2.4c) into the fourth-order differential operator yields

$$\begin{aligned} \frac{1}{\sin\phi}[W_D]w_m(\phi) &\equiv \sin^2\phi\frac{\partial}{\partial\phi}\sin\phi\frac{\partial}{\partial\phi}\frac{1}{\sin\phi}\frac{\partial}{\partial\phi}\sin\phi\frac{\partial}{\partial\phi}\left[\sum_{n=1}^{N} w_{n,m}\sin\phi\sin n\phi\right]\\ &= \sum_{n=1}^{N}[C_1(n)w_{n-4,m} - C_2(n)w_{n-2,m} + C_3(n)w_{n,m}\\ &\quad - C_4(n)w_{n+2,m} + C_5(n)w_{n+4,m}]\sin n\phi, \end{aligned} \quad (2.16)$$

where the polynomials $C_i(n)$ are

$$\begin{aligned} C_1(n) &= [(n-3)^2(n-2)^2]/16,\\ C_2(n) &= [2(n-3)(n-2)^3 + (n-2)(n-1)(n)(n+1) + (n-1)^2(n)(n+2)]/16,\\ C_3(n) &= [(n-3)(n-2)^2(n-1) + 2(n-2)(n)^2(n+1)\\ &\quad + (n+1)(n+2)^2(n+3) + 2(n+2)(n)^2(n-1)]/16,\\ C_4(n) &= [2(n+3)(n+2)^3 + (n+2)(n+1)(n)(n-1) + (n+1)^2(n)(n-2)]/16,\\ C_5(n) &= [(n+3)^2(n+2)^2]/16. \end{aligned} \quad (2.17)$$

The differential operator W_L is also found in (2.2). Operations for the remaining terms give

$$\begin{aligned} \frac{1}{\sin\phi}[W_S + W_L]w_m(\phi) &\equiv \frac{1}{\sin\phi}[W_S + W_L]\sum_{n=1}^{N} w_{n,m}\sin\phi\sin n\phi\\ &= \sum_{n=1}^{N}[F_1(n)w_{n-2,m} - F_2(n)w_{n,m} + F_3(n)w_{n+2,m}]\sin n\phi, \end{aligned} \quad (2.18)$$

$$F_1(n) = [(n-3)(n-2) + (n-1)(n)]/4,$$
$$F_2(n) = [(n-2)(n+1) + (n+2)(n-1) + 2n^2]/4,$$
$$F_3(n) = [(n+3)(n+2) + (n+1)(n)]/4,$$

and

$$\frac{1}{\sin\phi}[W_A]w_m(\phi) = \sin^3\phi \sum_{n=1}^{N} w_{n,m} \sin\phi \sin n\phi$$
$$= \frac{1}{16}\sum_{n=1}^{N}[w_{n-4,m} - 4w_{n-2,m} + 6w_{n,m} - 4w_{n+2,m} + w_{n+4,m}] \sin n\phi. \tag{2.19}$$

For negative indices, the sign of the spectral coefficients must be reversed, as in the case of the odd zonal wavenumber, and $w_{n,m} = 0$ for $n > N$.

2.2.3. *For* $\boldsymbol{m} = 0$

The operations for W_S and W_L are not necessary in this case. The result of expansion is the same as in the case of an odd zonal wavenumber except that the cosine series is used as the basis functions,

$$[W_D]w_0(\phi) \equiv \sin^3\phi \frac{\partial}{\partial\phi} \sin\phi \frac{\partial}{\partial\phi} \frac{1}{\sin\phi} \frac{\partial}{\partial\phi} \sin\phi \frac{\partial}{\partial\phi} \left[\sum_{n=0}^{N} w_{n,0} \cos n\phi\right]$$
$$= \sum_{n=0}^{N}[B_1(n)w_{n-4,0} - B_2(n)w_{n-2,0} + B_3(n)w_{n,0}$$
$$- B_4(n)w_{n+2,0} + B_5(n)w_{n+4,0}] \cos n\phi, \tag{2.20}$$

$$[W_A]w_0(\phi) = \frac{1}{16}\sum_{n=0}^{N}[w_{n-4,0} - 4w_{n-2,0} + 6w_{n,0} - 4w_{n+2,0} + w_{n+4,0}] \cos n\phi, \tag{2.21}$$

where the polynomials $B_i(n)$ are given in (2.12). As illustrated in the Appendix of [2], the even modes of $m = 0$ are solved by incorporating the Legendre polynomials (see the end of Section 3). Unlike cases where $m \neq 0$, negative indices of spectral coefficients should be replaced by positive indices with the same sign, such that

$$\begin{aligned} w_{-3,0} &\rightarrow w_{3,0}, \\ w_{-1,0} &\rightarrow w_{1,0}, \end{aligned} \tag{2.22}$$

which is attributed to the symmetric nature of cosine functions used as orthogonal functions.

2.2.4. *Linear Algebraic Equations with Pentadiagonal Matrices*

Using the orthogonality of the basis functions, Eq. (2.9) can be rewritten as algebraic equations with pentadiagonal matrices, such as (2.8), by equating the coefficients for each basis function of both sides. Note that operators W_L and W_S contribute only to the tridiagonal elements while operators W_D and W_A contribute to the pentadiagonal elements. The

structure of matrices Z and S, having only pentadiagonal elements, is expressed as

$$Z \equiv \begin{bmatrix} c_1 & d_1 & e_1 & & & & & \\ b_1 & c_2 & d_2 & e_2 & & & & \\ a_1 & b_2 & c_3 & d_3 & e_3 & & & \\ & a_2 & b_3 & c_4 & d_4 & e_4 & & \\ & & \ddots & \ddots & \ddots & \ddots & \ddots & \\ & & & & \ddots & \ddots & \ddots & \ddots \\ & & & & & \ddots & \ddots & \ddots \end{bmatrix}, \quad S \equiv \begin{bmatrix} x_1 & y_1 & z_1 & & & & & \\ q_1 & x_2 & y_2 & z_2 & & & & \\ h_1 & q_2 & x_3 & y_3 & z_3 & & & \\ & h_2 & q_3 & x_4 & y_4 & z_4 & & \\ & & \ddots & \ddots & \ddots & \ddots & \ddots & \\ & & & & \ddots & \ddots & \ddots & \ddots \\ & & & & & \ddots & \ddots & \ddots \end{bmatrix}.$$

Following the procedures described in Section 2, as an example, we illustrate the matrix elements of Z for even zonal wavenumbers other than zero with odd n,

$$\begin{aligned} a_i &= h_i + \gamma C_1(2i+3) && \text{for} \quad i \geq 1, \\ b_i &= q_i + \gamma[-C_2(2i+1) - m^2 F_1(2i+1)] && \text{for} \quad i \geq 2, \\ c_i &= x_i + \gamma[C_3(2i-1) + m^2 F_2(2i-1) + m^4] && \text{for} \quad i \geq 2, \\ d_i &= y_i + \gamma[-C_4(2i-1) - m^2 F_3(2i-1)] && \text{for} \quad i \geq 2, \\ e_i &= z_i + \gamma C_5(2i-1) && \text{for} \quad i \geq 1, \\ b_1 &= q_1 + \gamma[-C_1(3) - C_2(3) - m^2 F_1(3)], \\ c_1 &= x_1 + \gamma[C_2(1) + C_3(1) + m^2 F_1(1) + m^2 F_2(1) + m^4], \\ d_1 &= y_1 + \gamma[-C_1(1) - C_4(1) - m^2 F_3(1)], \end{aligned}$$

where the elements of S are given as

$$\begin{aligned} h_i &= 1/16 \quad \text{for} \quad i \geq 1, & q_i &= -4/16 \quad \text{for} \quad i \geq 2, \\ x_i &= 6/16 \quad \text{for} \quad i \geq 2, & y_i &= -4/16 \quad \text{for} \quad i \geq 2, \\ z_i &= 1/16 \quad \text{for} \quad i \geq 1, & q_1 &= -5/16, \\ x_1 &= 10/16, & y_1 &= -5/16. \end{aligned}$$

The pentadiagonal matrices are inverted with efficiency, but this requires computational operations which are about twice the number necessary for inversion of tridiagonal matrices. Therefore, computational efficiency of the BiHSF is enhanced by a factor of two, compared to the mixed-order HSF in (1.1).

3. HIGH-ORDER HARMONIC SPECTRAL FILTERS

High-order HSFs with order higher than 2 can be constructed in a way similar to that shown in the previous section. The third-order filter is equivalent to the inversion of the heptadiagonal matrices equation. An increase of one order in the harmonic filter brings about an increase in the number of diagonal bands by 2. Though feasible, the formulation of heptadiagonal or denser matrices associated with the third-order or higher HSF is a formidable task, requiring a repetition of the differentiation and multiplication illustrated in the Appendix. Direct construction of a complicated band-diagonal matrix can be avoided by introducing the operator-splitting method, which allows one to split the high-order harmonic

operator into first- and second-order hamonic equations. For example,

$$[1-\nu\nabla^6]X = [1-\gamma\nabla^2][1+\gamma\nabla^2+\gamma^2\nabla^4]X, \tag{3.1}$$

$$[1+\nu\nabla^8]X = [1+\sqrt{2}\gamma\nabla^2+\gamma^2\nabla^4][1-\sqrt{2}\gamma\nabla^2+\gamma^2\nabla^4]X, \tag{3.2}$$

$$[1-\nu\nabla^{10}]X = [1-\gamma\nabla^2][1+b\gamma\nabla^2+\gamma^2\nabla^4][1+c\gamma\nabla^2+\gamma^2\nabla^4]X, \tag{3.3}$$

$$[1+\nu\nabla^{12}]X = [1+\gamma^2\nabla^4][1+\sqrt{3}\gamma\nabla^2+\gamma^2\nabla^4][1-\sqrt{3}\gamma\nabla^2+\gamma^2\nabla^4]X, \tag{3.4}$$

where $\gamma = \nu^{1/q}$ with q is the order of the Laplacian, as in ∇^{2q}, and

$$b = \frac{1+\sqrt{5}}{2}, \quad c = \frac{1-\sqrt{5}}{2}. \tag{3.5a,b}$$

For convenience, the filters that incorporate operators (3.1)–(3.4) are called filter type III, IV, V, and VI, respectively. It is noted that the coefficient of the second-order harmonic term in the split equation (i.e., the right-hand-side) is always positive, as it should be. The coefficient of the first-order term in the second-order harmonic equations must satisfy that

$$\gamma_1^2 - 4\gamma < 0 \tag{3.6}$$

for

$$[1+\gamma_1\nabla^2+\gamma\nabla^4]X = Y; \quad \gamma > 0. \tag{3.7}$$

This necessary condition for filter coefficients can be obtained through the following "eigenvalue consideration." If the eigenvalue of the Laplacian operator is given as l_e, with l_e being a nonpositive integer, the eigenvalue of the filter operator in (3.7) is

$$1 + \gamma_1 l_e + \gamma l_e^2, \tag{3.8}$$

which should be positive for any l_e, and this requirement is satisfied by (3.6). (More details are presented in the next section.) It was found that violation of the condition causes a numerical overflow at the time of inverting the pentadiagonal matrices associated with (3.7). It is worth noting that the second-order harmonic equations in (3.1)–(3.4) all satisfy the condition in (3.6).

Spectral filtering with the high-order harmonic operator, as in (3.1)–(3.4), can be performed in terms of the inversion of the pentadiagonal (and tridiagonal) matrices. The pentadiagonal matrices in relation to the general second-order harmonic filter included in (3.1)–(3.4) can be formulated by adding additional elements to those derived in the previous section. The derivation of additional terms are described briefly. As in the previous section, the general second-order harmonic equation is multiplied by $\sin^4\phi$:

$$\sin^4\phi[1+\gamma_1\nabla^2+\gamma\nabla^4]w = g(\lambda,\phi)\sin^4\phi. \tag{3.9}$$

Thus, the additional terms that must be put into (2.9) are

$$\gamma_1\left[W_U - m^2 W_A^{1/2}\right]w_m(\phi), \tag{3.10}$$

where

$$\begin{aligned} W_U &= \sin^3\phi\frac{\partial}{\partial\phi}\sin\phi\frac{\partial}{\partial\phi} \\ &\equiv W_A^{1/2}W_L. \end{aligned} \tag{3.11}$$

The operator $W_A^{1/2}$ brings about the matrix A and W_U yields a pentadiagonal matrix

corresponding to AD when they are expanded with (2.4), where the matrices A and D are defined in (2.5). The results of applying the operation W_U to the zonal Fourier transform of $w_m(\phi)$ are presented for three categories:

(i) For odd $\boldsymbol{m}$,

$$[W_U]w_m(\phi) = \sum_{n=1}^{N}[-G_1(n)w_{n-4,m} + G_2(n)w_{n-2,m} - G_3(n)w_{n,m} + G_4(n)w_{n+2,m} - G_5(n)w_{n+4,m}]\sin n\phi, \tag{3.12}$$

$$\begin{aligned} G_1(n) &= [(n-4)(n-3)]/16, \\ G_2(n) &= [(n-3)(n-2) + 3(n-2)(n-1)]/16, \\ G_3(n) &= [3(n-1)(n) + 3(n+1)(n)]/16, \\ G_4(n) &= [(n+3)(n+2) + 3(n+2)(n+1)]/16, \\ G_5(n) &= [(n+4)(n+3)]/16. \end{aligned} \tag{3.13}$$

(ii) For even $\boldsymbol{m}(\neq 0)$,

$$\frac{1}{\sin\phi}[W_U]w_m(\phi) = \sum_{n=1}^{N}[-H_1(n)w_{n-4,m} + H_2(n)w_{n-2,m} - H_3(n)w_{n,m} + H_4(n)w_{n+2,m} - H_5(n)w_{n+4,m}]\sin n\phi, \tag{3.14}$$

$$\begin{aligned} H_1(n) &= [(n-3)(n-2)]/16, \\ H_2(n) &= [2(n-2)^2 + 2(n-1)(n)]/16, \\ H_3(n) &= [(n-2)(n-1) + (n+2)(n+1) + 4(n)^2]/16, \\ H_4(n) &= [2(n+2)^2 + 2(n+1)(n)]/16, \\ H_5(n) &= [(n+3)(n+2)]/16. \end{aligned} \tag{3.15}$$

(iii) For $\boldsymbol{m} = 0$,

$$[W_U]w_m(\phi) = \sum_{n=0}^{N}[-G_1(n)w_{n-4,m} + G_2(n)w_{n-2,m} - G_3(n)w_{n,m} + G_4(n)w_{n+2,m} - G_5(n)w_{n+4,m}]\cos n\phi. \tag{3.16}$$

The negative indices for $w_{n,m}$ are treated in the same way as in (2.15) and (2.22). Again, the even modes of $m = 0$ are solved by incorporating Legendre polynomials [2]. To do this, we construct an upper triangular matrix L_{ij} of which elements are given by the following (in double precision FORTRAN code).

```
   a(0)= 1.d0
do i=1,N
   a(i)= a(i-1)*(2.d0*i-1)/(2.d0*i)
end do
do j=0,N/2
   L(0,j)= a(j)**2
do i=1,j
   L(i,j)= a(j-i)*a(j+i)*2.d0
end do
end do
```

We first obtain the solution of the matrix equation $L\boldsymbol{u} = \boldsymbol{g}$, where $\boldsymbol{g}$ is a column vector consisting of the spectral expansion coefficients of the forcing function $g(\lambda, \phi)$ for the even mode of $m = 0$ as in Eq. (3.9). Then, filtering is accomplished by $w_{2i,0} = \sum_{j=i}^{N/2} L_{ij} u_j (1 + \gamma_1 l_e + \gamma l_e^2)^{-1}$ for $i = 0, 1, \ldots, N/2$ with $l_e = -2j(2j + 1)$.

4. ACCURACY AND PERFORMANCE OF THE HIGH-ORDER HARMONIC SPECTRAL FILTER

The operation count necessary for the HSF is nearly proportional to the order of the filter. For example, if the operations needed for filter type IV is N_f, type II and VI filters need $0.5N_f$ and $1.5N_f$, respectively, and filter type IIA requires nearly the same operations as those for IV. In this section, the accuracy and performance of the high-order HSF are evaluated in comparison with the filter used in [2]. The relative performance of the high-order HSF, except for the type IIA filter used in [2], as measured in terms of scale selectivity, is easily understood: A sharper cutoff can be achieved as the order increases. Therefore, for certain test cases shown below, the performance comparison of the various filter types is restricted to filters type II (BiHSF) and IIA. We take four cases into consideration. All computations for the cases were carried out with double precision (providing the floating points of 15 digits), using a DIGITAL FORTRAN 90 compiler on a DIGITAL UNIX Alpha system.

4.1. Response Function of the Biharmonic Spectral Filter

In this section, the performance of the filter is presented in terms of response to a scale-defined function, as was done in [2]. The functions to be used are the eigenfunctions of the matrix $[A^{-1}D]$ for each zonal wavenumber, as was done in [1], which is the discrete form of the harmonic operator. The zonal and meridional wavenumber truncations are set at $M = N = 64$ for the eigensystem; the size of $[A^{-1}D]$ is 32×32 because the hemispherically symmetric and antisymmetric modes are calculated separately. Let $Q_{l^*}^m$ be the eigenfunction for the zonal wavenumber m and meridional mode number l^*. As was shown in [1] the eigenfunctions with $l^* + m \leq M$ are exactly the same as the associated Legendre functions, for which the eigenvalues l_e are given as $-(l^* + m)(l^* + m + 1)$. The response function, defined as the amplitude ratio $R = (Q_{l^*}^m)^f / Q_{l^*}^m$ of the BiHSF, is presented in Fig. 1 in

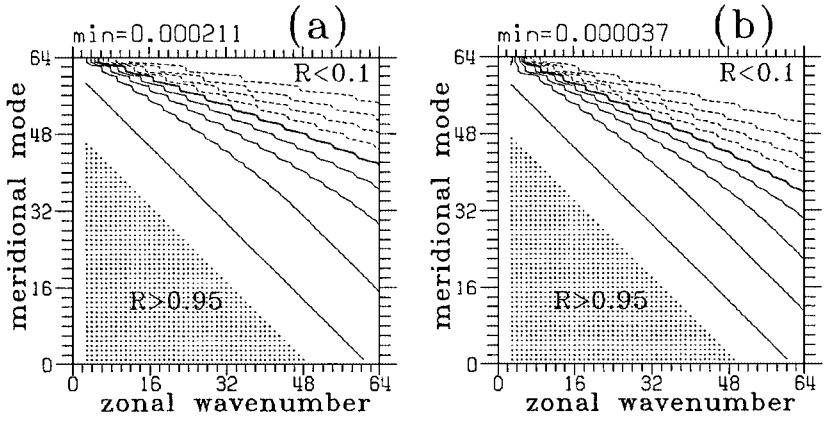

FIG. 1. The response of the filter, defined as the amplitude ratio $R = (Q_{l^*}^m)^f / Q_{l^*}^m$, where $Q_{l^*}^m$ is the eigenfunction of the Laplacian, with m and l^* the zonal and meridional mode numbers, respectively. (a) Filter type IIA in Eq. (1.1). (b) Filter type II. Filter viscosities for (a) and (b) are 0.643×10^{-4} and 0.784×10^{-8}, respectively. (Solid and dashed lines) $R \geq 0.5$ and $R < 0.5$, respectively; (thick solid line) $R = 0.5$.

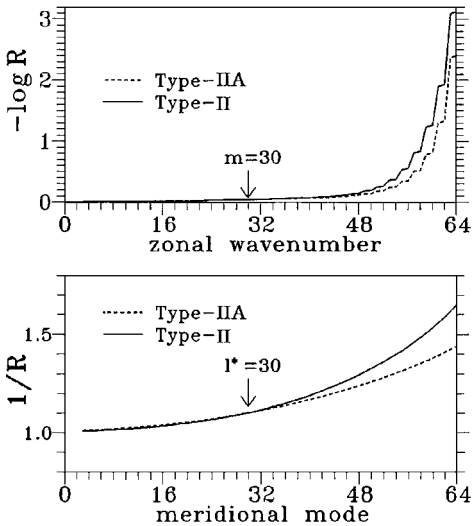

FIG. 2. Cross sections of Fig. 1 for $m = 30$ (upper panel) and $l^* = 30$ (lower panel). Type IIA refers to the mixed-order harmonic spectral filter in Eq. (1.1). Type II is the biharmonic spectral filter. (Arrow) The point at which the responses of both filters are the same.

comparison with that of the filter defined in (1.1). The filter coefficients are determined in such a way that the amplitude ratio for $(l^*, m) = (30, 30)$ becomes 0.905 for both filters. The results in Fig. 1 remain the same for the wavenumbers $l^* + m \leq M$ even though a different resolution is used. On the other hand, they may vary for other, higher wavenumbers $(l^* + m > M)$ but the qualitative features must be unchanged, because the eigenvalues of the matrix $[A^{-1}D]$ exhibit a systematic distribution, as is shown in Fig. 1 of [2].

As a whole the response functions of two filters are very similar to each other. As was noted in [2], the response increases (that is, R decreases) with m and l^*, and the same response is achieved at the same value of $(l^* + m)$ for $l^* + m \leq M$. Stepwise variation of the response is found at a large l^* for $l^* + m > M$. One can clearly identify that the response of the BiHSF is stronger than that of the type IIA filter by noticing that the thick line of $R = 0.5$ for the former shifted below compared to that for the latter. To see more clearly how the responses differ from each other, cross sections passing over $(l^*, m) = (30, 30)$ of Fig. 1 are shown in Fig. 2. For better visualization, the ordinate represents $-\log R$ in the upper panel and $1/R$ in the lower. The arrows indicate the zonal wavenumber of meridional mode number at which the responses exhibit the same values. On the left side of the arrow, the response for the type IIA filter is larger than that for type II, while this is reversed on the right side. It is worth noting that the type II filter dampens down the high-wavenumber components more effectively than the filter in (1.1) in spite of being composed of only the second-order hamonic operator. This is the very desirable property we expected the new filter to have. The better performance of the type II over the type IIA filter is a consequence of the fact that it directly inverts the pentadiagonal matrix, instead of carrying out multiple inversions of the tridiagonal matrix and introducing an auxiliary operation.

Since the eigenvectors are the same as the associated Legendre functions for $l^* + m \leq M$, the response must be identical to the theoretical value:

$$R_t = \left(1 + \gamma l_e^2\right)^{-1}. \tag{4.1}$$

TABLE I

Normalized Error of the Filter's Response to Eigenfunctions of the Laplacian for $l^* + m \leq M$, Where m and l^* Are the Zonal Wavenumber and Mode Number

Mode number	$m = 31$ (odd)	$m = 31$ (even)	$m = 32$ (odd)	$m = 32$ (even)
1	0.2238E−15	0.1792E−14	−0.1120E−15	0.1346E−14
2	−0.6730E−15	0.3369E−15	0.2246E−15	0.2924E−14
3	−0.3374E−15	0.2140E−14	0.6758E−15	0.3384E−15
4	−0.4512E−15	−0.1017E−14	0.9041E−15	−0.1812E−14
5	−0.6793E−15	−0.6807E−15	0.1361E−14	−0.1251E−14
6	0.5685E−15	−0.2279E−15	0.0000E+00	−0.4570E−15
7	−0.4570E−15	−0.1375E−14	0.1146E−14	−0.2298E−15
8	−0.4596E−15	0.1152E−15	0.6915E−15	−0.3469E−15
9	0.1272E−14	−0.1044E−14	−0.2320E−15	0.3493E−15
10	0.1164E−15	−0.1987E−14	−0.2338E−15	0.4695E−15
11	−0.5869E−15	−0.5894E−15	0.0000E+00	−0.7105E−15
12	0.5921E−15	−0.2380E−15	−0.4760E−15	−0.1196E−15
13	0.0000E+00	−0.7214E−15	−0.4809E−15	0.7254E−15
14	0.6045E−15	−0.2432E−15	−0.6080E−15	−0.6117E−15
15	−0.1223E−15	−0.3694E−15	−0.1354E−14	−0.7437E−15
16	−0.1116E−14	−0.8737E−15	−0.1123E−14	0.3771E−15
17	−0.5029E−15	0.5066E−15	−0.6333E−15	−0.6383E−15

The response error of the BiHSF, defined as

$$\frac{R - R_t}{R_t}, \tag{4.2}$$

is evaluated for $m = 31$ and 32. It is found that the errors for all meridional modes fall within the order of machine rounding $O(10^{-15})$ or less, as shown in Table I, indicating that the pentadiagonal matrices can be inverted with accuracy.

4.2. Test of the Isotropic Nature of the Filter

Since the filter is applied to the variables defined on the spherical surface, it is required that it be isotropic. That is, the response of the filter to a field variable over a sphere should not be dependent on the rotation of the field. This is trivially satisfied for the spectral filter with a spherical harmonics basis (see, for example, [3, 4, 5, 8, 9]) because spherical harmonics are isotropic. On the other hand, this is not the case for other filters. To test this property we set a bell-shaped field variable centered at $(0, \phi_0)$ as

$$g(\lambda, \phi) = \exp\{-(r/r_0)^2\}, \tag{4.3}$$

where r is the arclength measured along the great circle from $(0, \phi_0)$ and γ_0 is the scale parameter fixed as $\pi/20$. The center is determined to be located over a grid point. We transform $g(\lambda, \phi)$ into the spectral space, then apply the filter to it. In this case, $M = 128$, N is 127 (128) for $m = 0$ ($m \neq 0$), and the transform grids are set at 256×128. ($M = K/2$ and $N = M - 1(M)$ for $m = 0$ ($m \neq 0$) with the transform grids of $K \times K/2$ constitutes the *full wave resolution* when the interior grid system is adopted in the double Fourier series [1, 2].)

Two quantities are calculated for the error evaluation: One is the global-mean error of the filtered field, normalized by the reference field $g_c(\lambda, \phi)$, of which the center is $(0, \Delta\phi/2)$

TABLE II

Normalized Error of the Filter's Response to a Bell-Shaped Field Variable Defined as in (4.3), Where ϕ_0 Denotes the Center and $\Delta\phi = \pi/128$

ϕ_0	ε^a	Error of grid-point value
20.5 $\Delta\phi$	3.529E−11	−3.129E−16
32.5 $\Delta\phi$	7.676E−11	9.388E−16
42.5 $\Delta\phi$	4.721E−11	−7.824E−16
62.5 $\Delta\phi$	2.366E−10	−4.694E−14

[a] Definition given in (4.4).

with $\Delta\phi = \pi/128$,

$$\varepsilon = \frac{[|g^f|] - \left[\left|g_c^f\right|\right]}{\left[\left|g_c^f\right|\right]}, \tag{4.4}$$

where the superscript and square brackets denote the filtered variable and global mean, respectively. The other is the grid-point value error at $g^f(\lambda, \phi) = g^f(0, \phi_0 - 5\Delta\phi)$, normalized by the reference value, i.e., $g_c^f(0, \Delta\phi/2)$. The results for four different locations are illustrated in Table II. The global-mean error falls within $O(10^{-11})$ or $O(10^{-10})$, and it is largest for the case where the center is located near the North Pole. The normalized error of a grid-point value slightly increases as the field is rotated poleward, but it remains $O(10^{-14})$ even in the worst case.

4.3. Application to a Time-Dependent Nonlinear Flow

In this section, the spectral filter is used as an implicit diffusion to a time-dependent nonlinear vorticity equation on a sphere. The vorticity equation, scaled by the radius and rotation rate of the earth, is written as

$$\frac{\partial \zeta}{\partial t} = \frac{-1}{\sin^2\phi}\left[\frac{\partial}{\partial\lambda}U\eta + \sin\phi\frac{\partial}{\partial\phi}V\eta\right] + F, \tag{4.5}$$

where $\eta = f + \zeta$, with f being the Coriolis parameter and F being the viscosity. $U \equiv u \sin\phi$ and $V \equiv v \sin\phi$, with u and v being the longitudinal and latitudinal components of the velocities, respectively. Using a leapfrog scheme for time differentiation, the vorticity equation can be time-marched with implicit time-stepping with respect to the viscosity term as

$$[1 + \gamma\nabla^4]\zeta^{(p+1)} = \zeta^{(p-1)} + 2\Delta t J^{(p)} \tag{4.6}$$

in the case of biharmonic viscosity (or filter type II), $F = -\nu\nabla^4\zeta$, or

$$[1 - \gamma\nabla^2]^3\zeta^{(p+1)} = \zeta^{(p-1)} + 2\Delta t J^{(p)} - 3\gamma\nabla^2\zeta^{(p-1)} \tag{4.7}$$

in the case of mixed-order harmonic viscosity (*or* filter type IIA), $F = -\alpha\nabla^4\zeta + \beta\nabla^6\zeta$, where J is the advection term. The implicit treatment of viscosity allows one to take a large time step, regardless of the magnitude of the viscosity (cf. [2, 5]). Superscripts $(p-1)$, (p),

and $(p + 1)$ indicate past, present, and future time step, respectively. Through spectral expansion of the dependent variables, (4.6) and (4.7) are replaced by linear algebraic equations for each set of unknown spectral coefficients at the $(p + 1)$ time step. When the spectral coefficients of variables at the $(p - 1)$ and (p) time steps are given, quadruple inversions of tridiagonal matrices are needed for the solution of (4.7). However, a single inversion of the pentadiagonal matrices is sufficient to solve (4.6) for each set of spectral coefficients.

As in [2], one can readily determine the filter viscosity in (4.6) just by specifying the damping rate of a certain scale. For example, if we want to give the damping rate of the total wavenumber N as $1/(5$ days), the filter viscosity for the BiHSF must be given as $\gamma = 2\Delta t/[(5\text{days}) \cdot N^2(N + 1)^2]$. To determine an appropriate value for the viscosity in the case of an explicit viscosity is not always easy for the numerical methods which do not adopt the longitude–latitude coordinate system (e.g., [10]), probably due to the unavailability of the stability condition for the diffusion equation with the Laplacian operator (that is, something like CFL criteria).

In this section we simulate the barotropic instability of the zonal-mean flow with double shear zones, which is of hemispheric symmetry. The initial zonal-mean flow and absolute vorticity of the northern hemisphere are shown in Fig. 3. One of the shear zones is located around 25° and the other is located around 60° in both hemispheres. As is shown below, the zonal-mean shear flow is unstable, so the small-amplitude perturbations superimposed on it will have grow exponentially in the initial stage. The growing modes at the two shear zones will have similar zonal scales because the strength of the shears are similar to each other, which implies that the zonal wavenumber of the most unstable mode over one shear zone is different from that of the other. Thus, the global normal mode of a single zonal wavenumber for the unstable zonal-mean flow [10] is not very useful in this study. Considering this fact, for simplicity the initial field is perturbed by adding small perturbations to the shear zones, with the maximum over the center of the shear zone and decreasing exponentially away from the center. The perturbation of hemispheric asymmetry consists of zonal wavenumbers 1–20, and the amplitude of each zonal wavenumber component is kept at 1% of the maximum absolute vorticity. Numerical experiments are carried out for four cases, whose parameters are summarized in Table III. The viscosities for EXP-C and -D are very close to each other. The reason for this is to demonstrate that the flow is so strongly nonlinear that the decrease rate of the total kinetic energy (TKE) fluctuates with time and at a certain stage the weak viscosity case maintains rather a larger TKE level than the strong viscosity case. Be careful

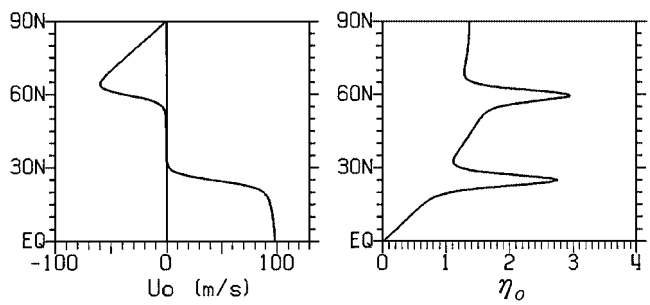

FIG. 3. Initial profile of the zonal-mean flow (left panel) and the absolute vorticity (right panel) used for the simulation of barotropic instability of the doubly sheared flow. The absolute vorcity is nondimensional, i.e., scaled by Earth's rotation rate.

TABLE III
Parameters for Numerical Experiments on Barotropic Instability of Zonal-Mean Flow with Double Shear Zones

	$M(=N)$	Δt (s)	Number of grids	Filter type	Filter viscosity (γ)
EXP-A	170	240	512×256	II	6.57×10^{-11}
EXP-B	340	72	1024×512	II	9.19×10^{-12}
EXP-C	170	240	512×256	IIA	5.23×10^{-6}
EXP-D	170	240	512×256	IIA	5.41×10^{-6}

that the filter viscosities for EXP-C and -D are not compared to that of EXP-A. Rather, the viscosity coefficient for the second-order harmonic operator of the original mixed-order diffusion equation must be compared to it.

Before discussing the performance of the filter in terms of TKE loss due to viscosity (*or* the filter), we illustrate in Fig. 4 the northern polar stereographic projection of the absolute vorticity at selected days in the case of EXP-B. Since it is not the main concern, we do not pay attention to the detailed dynamic features of the flow. The time evolution of the flow field, as inferred from the vorticity field, is characterized by the exponential growth of unstable waves, the saturation and the generation of isolated vortices, the merger and breaking of them, and, finally, the formation of a coherent vortex. We could not find noiselike small scales in these maps, implying a satisfactory performance of the BiHSF.

In Fig. 5 we present the time variation of TKE loss normalized by the initial value for four cases. TKE monotonically decreases with time due to viscosity, and the TKE loss at day 50 remains smaller than 10^{-2} for all cases. For the experiment with doubled model resolution, TKE loss is maintained at several times smaller than those of the remaining cases, because of reduced viscosity. Obviously, TKE loss for EXP-C and -D is less than that of EXP-A at day 50, but this does not reflect the relative accuracy of the filters, as we can control TKE loss by tuning the filter viscosity. It is worth noting that the TKE for EXP-A exhibits a rather small decrease rate during the first several days; however, it sharply decreases around day 10 and thereafter it becomes smaller than those for EXP-C and -D. This sharp decrease happens when the vortices, as a result of a strong interaction among them, break into the smaller scales accompanying the vortex filaments. Such an intersection of the TKE curves is a clear indication of the difference in the performance of the two types of filters. This confirms again the superiority of the BiHSF to the type IIA filter, as is demonstrated by the response characteristics shown in Figs. 1 and 2.

4.4. Application to Shallow-Water Equations with an Observed Flow

4.4.1. *Filter Response to an Observed Field Superimposed with Artificial Noise*

In this section, we apply the spectral filters to the observed flow and compare their performance in aspects of selective dampening at small scales. The seven types of filters, from type-I to -VI and -IIA, are compared to one another, where a full wave resolution for 256×128 transform grids is given. Type-I refers to the filter of a single Laplacian operator. Since the seven filters of interest are distinguished by the order of the harmonic operator, the absolute value of the filter coefficient does not have a strict meaning. So the appropriate filter viscosity must be sought in a systematic way. The procedure to specify filter viscosity

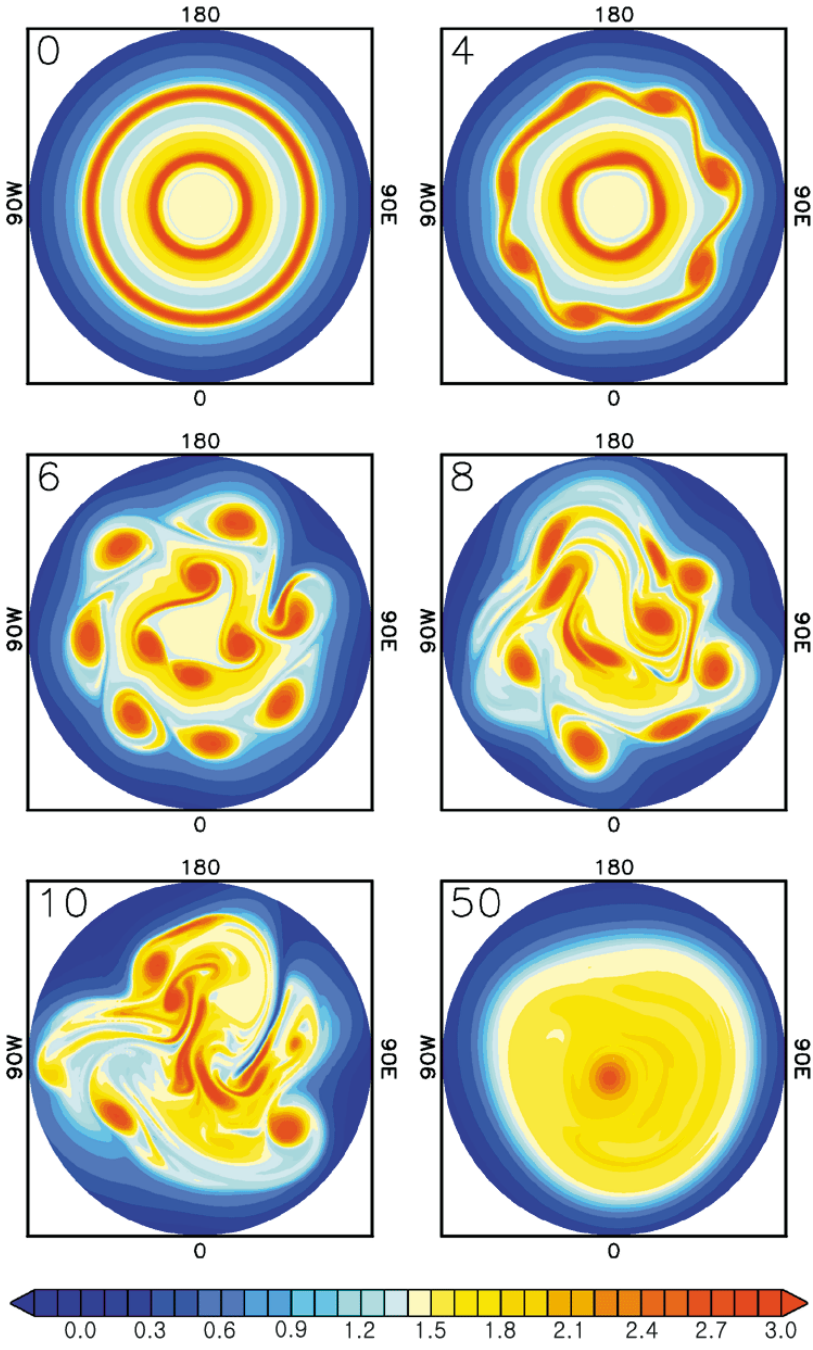

FIG. 4. The absolute-vorticity field at selected days for the numerical experiment on barotropic instability, where the numerals on the top left of each map denote time (day).

for a certain filter is as follows.

(i) Produce a geopotential perturbation which is confined to a very narrow region,

$$\Phi_N = \begin{cases} \Phi_0[1 + \cos(\pi r / r_m)]/2, & r \le r_m, \\ 0, & r > r_m, \end{cases} \tag{4.8}$$

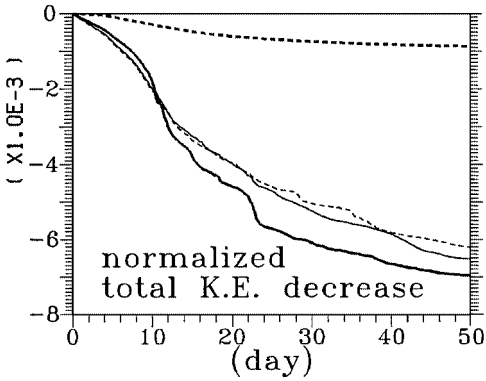

FIG. 5. The total-kinetic-energy decrease, normalized by the initial value, in the case of the numerical experiments on barotropic instability. The thick and thin solid lines correspond to EXP-A and EXP-C, respectively, and the thick and thin dashed line correspond to EXP-B and EXP-D, respectively.

where r is the arclength measured from the nearest grid point to $(\lambda, \phi) = (180°\text{E}, 10°\text{N})$ with $r_m = \pi/128$. The scale of the perturbation field corresponds to the two-grid length, being close to the smallest scale resolvable in the model. As the amplitude, Φ_0, the positive maximum value ($270.6 \times 9.8\ \text{m}^2\ \text{s}^{-2}$) of the geopotential field of 00Z 19 September 1999, with the global mean subtracted, is given.

(ii) Choose an arbitrary filter viscosity γ and apply the filter to the spectral space of Φ_N. If the maximum of the filtered field Φ_N^f is greater (smaller) than $0.05\Phi_0$, redefine the filter viscosity by increasing (reducing) by a small fraction of the previous value.

(iii) Repeat step ii until the maximum of the filtered field approaches $0.05\Phi_0$ with a small prescribed error.

We superimpose the geopotential perturbation produced by (4.8) on the observed geopotential field of the 500-hPa surface at 00Z 19 September 1999 from which the global mean is eliminated. Then the spectral filters are applied to this field, each with the filter viscosity obtained above. Some of the results are presented in Fig. 6; the contour label was omitted for clarity. The first map shows the unfiltered field, the observation plus the perturbation, with the perturbation centered at (180°E, 10.55°N) indicated by an arrow. The filtered field (thick dashed line) is overlapped on the unfiltered field (thin solid line) to see how the response is varied with the order of the harmonic filter. Since filter viscosity was carefully chosen to reduce the amplitude of the perturbation to 1/20 of the initial value, the perturbation seems to have disappeared. (The perturbation can be observed only in the thin solid line contours.)

It is worth noting that the dashed and solid lines almost overlap each other except in the regions of small-scale variations for type IIA and II filters. They become even more visibly indistinguishable over the global domain for type-IV. Not shown, the main features for type-V and -VI are nearly the same as those for type-IV. In other words, the high-order HSF can remove selectively the small-scale features without affecting the large-scale patterns. As a quantitative measure, we take the absolute value of the difference between the filtered and the initial field and then calculate its global average (Table IV),

$$\Lambda = [|\Phi^f - \Phi|], \tag{4.9}$$

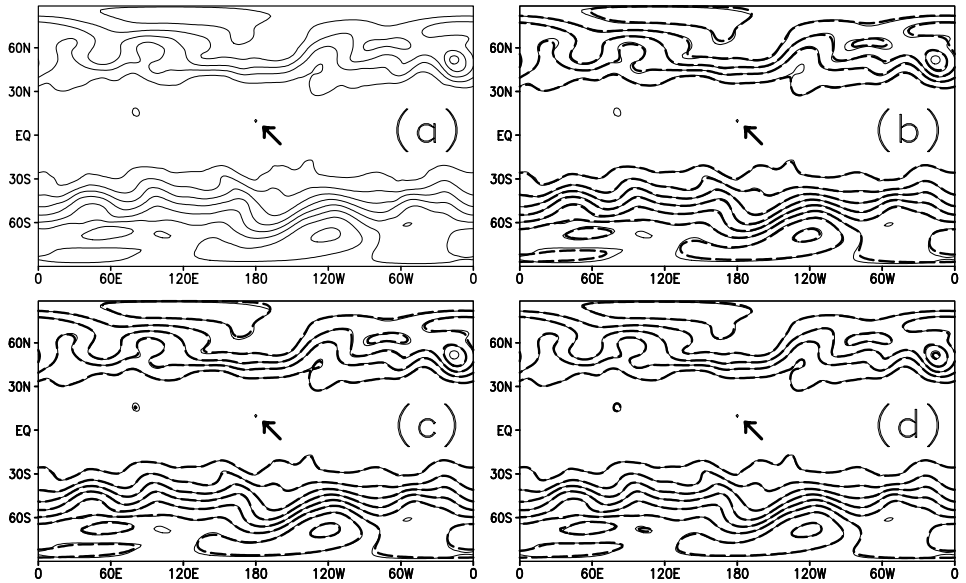

FIG. 6. Application of the harmonic filters to an observed geopotential field on which an artificial perturbation (arrow) defined in Eq. (4.8) is superimposed. The contour values range from -811.8×9.8 m^2 s^{-2} to 405.9×9.8 m^2 s^{-2} and are scaled by 135.3×9.8 m^2 s^{-2}. Solid and dashed lines denote unfiltered and filtered fields, respectively. Unfiltered field (a). Filtered by type IIA (b), type II (c), and type IV (d). The small-scale artificial perturbation in b, c, and d are drawn in thin solid lines, which implies that it disappeared in the spectral filtering.

where the meaning of the symbols are the same as in (4.4). Λ exhibits a monotonic decrease as the order of the filters increases, with a sharp variation for type-I through type-IV and rather a slow decrease rate beyond type IV. It should be emphasized that type IIA shows a larger value than type II, indicating that type IIA is actually a lower filter than type II although it contains a third-order harmonic operator. This confirms the results presented in the previous section.

TABLE IV

Global Average of the Difference between the Filtered and Unfiltered Field, with a Unit of 270.6×9.8 m^2 s^{-2}

Filter type[a]	Λ[b]
I	4.887E−02
IIA	1.583E−02
II	1.011E−02
III	0.639E−02
IV	0.558E−02
V	0.532E−02
VI	0.524E−02

[a] Filters types I through VI correspond to the order of the harmonic operator ∇^{2q}, and type IIA is represented by Eq. (1.1).

[b] Definition presented in Eq. (4.9).

4.4.2. *Harmonic Spectral Filtering in the Shallow-Water Equations*

The shallow-water equations consist of the vorticity equation in (4.5) and divergence and geopotential equation [2],

$$\frac{\partial \delta}{\partial t} = \frac{+1}{\sin^2\phi}\left[\frac{\partial}{\partial \lambda} V\eta - \sin\phi \frac{\partial}{\partial \phi} U\eta\right] - \nabla^2\left[\Phi' + \frac{U^2+V^2}{2\sin^2\phi}\right], \tag{4.10}$$

$$\frac{\partial \Phi'}{\partial t} = \frac{-1}{\sin^2\phi}\left[\frac{\partial}{\partial \lambda} U\Phi' + \sin\phi \frac{\partial}{\partial \phi} V\Phi'\right] - \bar{\Phi}\delta, \tag{4.11}$$

where the variables are scaled by the radius, a, and inverse rotation rate, Ω^{-1}, of the Earth, $\bar{\Phi}$ is the time-invariant global-mean geopotential and Φ' is the geopotential deviation from it, and δ is the divergence. The semiimplicit time-stepping is incorporated to suppress gravity-wave oscillation and thus to take a larger time-step size than the explicit method. The initial condition uses the observed 500-hPa surface data at 00Z 19 September 1999, of which the geopotential was also used in the previous section. For the vorticity equation the high-order implicit diffusion (i.e., HSF) can be used with ease. However, although possible, incorporating high-order implicit diffusion into divergence and geopotential equations requires a very complicated operation in cases where semiimplicit time-stepping is adopted. Therefore, we apply the filter to the predicted variables, as in [2].

We specify the filter viscosity in the same way as in the previous section, but in this case the amplitude reduction was set at 0.5 instead of 0.05. Transform grids of 256×128 and the wave truncation $M = N = 64$ are given here. The model is integrated for 100 days with a time-step size of 12 min, which is considered to be sufficient to figure out the performance of the spectral filters. The total energy decrease normalized by the initial value is presented in Fig. 7. Note that the total energy decreases at a large rate over a couple of 10-day periods, followed by a slow decrease rate. Unlike the vortex amalgamation problem simulated with the vorticity equation, the energy-decrease curves are very smooth, due to the rather weak nonlinear interactions among different scales. Clearly, energy loss is greatest for the lowest

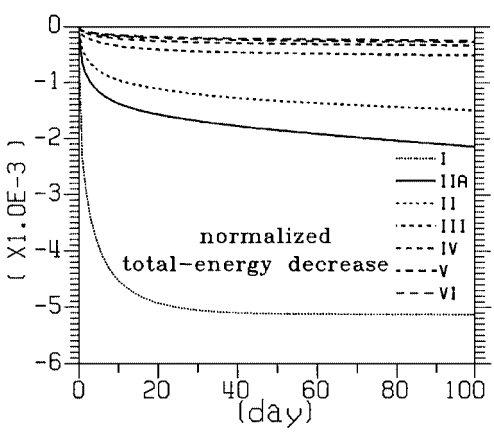

FIG. 7. Total energy decrease with time, normalized by the initial value, in the case of the observed flow of a 500-hPa surface at 00Z 19 September 1999. Transform grids and wave truncations are given by 256×128 and $M = N = 64$.

order filter and diminishes as order increases. However, for types IV, V, and VI harmonic filters, the energy-decrease tendency is very similar, not showing significant differences. From Fig. 7 it can be seen that the curve for type II runs between those of types I and II, implying again the superiority of type II over type IIA.

5. SUMMARY AND CONCLUSIONS

We implemented the high-order HSF up to the sixth order with the double Fourier series as orthogonal basis functions to smooth out a field variable defined on a spherical surface. The filter consists of solving the high-order harmonic diffusion equation using the implicit method. The high-order harmonic operators included in the filter are split into second-order and lower harmonic operators, and the second- (first-) order harmonic operator is replaced by a pentadiagonal (tridiagonal) matrix whose elements are the spectral coefficients. Then the high-order HSF performs filtering through successive inversions of the pentadiagonal or tridiagonal matrices. The accuracy, performance, and isotropic nature of the filter were tested in terms of responses to eigenvectors of the Laplacian operator, a bell-shaped field, and time-dependent flow. The main features of the high-order HSF are as follows.

(i) The error associated with the inversion of pentadiagonal matrices (or equivalently the high-order HSF) was found to be on the order of machine rounding.

(ii) The filter is isotropic so that its performance on a field variable is not affected by the poleward rotation.

(iii) Due to the direct invertibility of the pentadiagonal matrices, the BiHSF (filter type II) performs better than the mixed-order HSF (type IIA) used by [2] in the sense that it can provide a sharper cutoff of high wavenumbers in spite of the fact that type IIA has a higher harmonic operator than type-II.

(iv) The operation count associated with the filter is nearly proportional to the order of the filter, and the BiHSF needs only half of the operation count required for the type IIA filter.

(v) Filter viscosity can be readily determined just by specifying the dampening rate of a prescribed scale.

The results of the present study indicate that the high-order HSF will enhance stability and efficiency of the spectral model developed by [1, 2]. In addition to the key role as a numerical stabilizer for a predicting system, the filter can also be used for various problems with accuracy and efficiency as long as the problems concern the filtering (smoothing) out field variables defined over a spherical surface.

APPENDIX

Of the whole procedure involved in the derivation of (2.8), we show the first three steps because the following operations can also be done in a way similar to those. Here, we present an example for the case of an odd zonal wavenumber, where sine expansion in the meridional direction is necessary:

$$w(\phi) = \sum_{n=1}^{N} w_n \sin n\phi. \tag{A.1}$$

For simplicity, we drop the zonal wavenumber index. Differentiation of $w(\phi)$ with respect to ϕ and multiplication of $\sin\phi$ give

$$\begin{aligned}\sin\phi\frac{\partial}{\partial\phi}w(\phi) &= \sum_{n=1}^{N}(n)w_n\cos n\phi\sin\phi\\ &= \frac{1}{2}\sum_{n=1}^{N}(n)w_n[\sin(n+1)\phi-\sin(n-1)\phi]\\ &= \frac{1}{2}\sum_{n=1}^{N}[(n-1)w_{n-1}-(n+1)w_{n+1}]\sin n\phi, \end{aligned}\tag{A.2}$$

where the spectral coefficient with mode indices greater than N, or less than zero, must be retained until the last operation. Subsequent operations up to the third differentiation yield

$$\begin{aligned}&\sin\phi\frac{\partial}{\partial\phi}\frac{1}{\sin\phi}\frac{\partial}{\partial\phi}\sin\phi\frac{\partial}{\partial\phi}w(\phi)\\ &\quad=\frac{1}{2}\sum_{n=1}^{N}[(n-1)w_{n-1}-(n+1)w_{n+1}](n)\cdot\left[\frac{-(n)\sin n\phi\sin\phi-\cos n\phi\cos\phi}{\sin^2\phi}\right]\sin\phi\\ &\quad=\frac{1}{4}\sum_{n=1}^{N}[(n-1)w_{n-1}-(n+1)w_{n+1}](n)\\ &\qquad\cdot\left[\frac{-(n)\{\cos(n-1)\phi-\cos(n+1)\phi\}-\{\cos(n-1)\phi+\cos(n+1)\phi\}}{\sin\phi}\right]\\ &\quad=\frac{1}{4}\sum_{n=1}^{N}[(n-2)^2(n-1)w_{n-2}+(n+2)^2(n+1)w_{n+2}-\{(n-2)(n-1)(n)\\ &\qquad+(n+2)(n+1)(n)\}w_n]\frac{\cos n\phi}{\sin\phi}.\end{aligned}\tag{A.3}$$

For the present step, the three expansion coefficients $w_{n\pm2}$ and w_n are retained for each spectral expansion term. The remaining operations are the differentiations with respect to ϕ and the multiplication of $\sin^3\phi$ in order, which are carried out in a similar way to those shown above. In the final step, the five expansion coefficients $w_{n\pm4}$, $w_{n\pm2}$, and w_n remain for each $\sin n\phi$ term.

ACKNOWLEDGMENTS

This research was supported by KOSEF Grant KOSEF-2000-1-13400-001. The authors acknowledge the anonymous reviewers for their useful comments.

REFERENCES

1. H.-B. Cheong, Double Fourier series on a sphere: Applications to elliptic and vorticity equations, *J. Comput. Phys.* **157**, 327 (2000).
2. H.-B. Cheong, Application of double Fourier series to shallow water equations on a sphere, *J. Comput. Phys.* **165**, 261 (2000).

3. R. Jakob and B. K. Alpert, A fast spherical filter with uniform resolution, *J. Comput. Phys.* **136**, 580 (1997).
4. R. Jakob, J. Hack, and D. L. Williamson, Spectral transform solutions to the shallow water test set, *J. Comput. Phys.* **119**, 164 (1995).
5. M. N. Jukes and M. E. McIntyre, A high-resolution one layer model of breaking planetary waves in the stratosphere, *Nature* **328**, 590 (1987).
6. S. A. Orszag, Fourier series on spheres, *Mon. Weather Rev.* **102**, 56 (1974).
7. C. Ronchi, R. Iacono, and P. S. Paolucci, The "cubed sphere": A new method for the solution of partial differential equations in spherical geometry, *J. Comput. Phys.* **124**, 93 (1996).
8. A. J. Simmons and B. J. Hoskins, The life cycles of some nonlinear baroclinic waves, *J. Atmos. Sci.* **35**, 414 (1978).
9. W. F. Spotz, M. A. Taylor, and P. N. Swartztrauber, Fast shallow water equation solvers in latitude–longitude coordinates, *J. Comput. Phys.* **145**, 432 (1998).
10. G. R. Stuhne and W. R. Peltier, Vortex erosion and amalgamation in a new model of large scale flow on the sphere, *J. Comput. Phys.* **128**, 58 (1996).
11. M. A. Taylor, J. Tribbia, and M. Iskandarani, The spectral element method for the shallow water equations on the sphere, *J. Comput. Phys.* **130**, 92 (1997).